Continuous-Wave Second-Harmonic Generation in Orientation-Patterned Gallium Phosphide Waveguides at Telecom Wavelengths: Supporting Info

Konstantinos Pantzas,[*,†] Sylvain Combrié,[‡] Myriam Bailly,[†,‖] Raphaël Mandouze,[‡] Francesco Rinaldo Talenti,[‡,⊥] Abdelmounaim Harouri,[†] Bruno Gérard,[¶] Grégoire Beaudoin,[†] Luc Le Gratiet,[†] Gilles Patriarche,[†] Alfredo De Rossi,[‡] Yoan Léger,[§] Isabelle Sagnes,[†] and Arnaud Grisard[‡]

†*Centre de Nanosciences et de Nanotechnologies, CNRS, Université Paris Saclay,91120 Palaiseau, France*

‡*Thales Research and Technology, Campus Polytechnique, 1 avenue Augustin Fresnel, 91767 Palaiseau, France*

¶*III-V Lab, Campus Polytechnique, 1 avenue Augustin Fresnel, 91767 Palaiseau, France*

§*Institut Foton (UMR6082/CNRS-Univ. Rennes-INSA), 20 avenue des Buttes de Coësmes, 35708 Rennes, France*

‖*Thales Research and Technology, Campus Polytechnique, 1 avenue Augustin Fresnel, 91767 Palaiseau, France*

⊥*Dipartimento di Ingegneria dell'Informazione, Elettronica e Telecomunicazioni, Sapienza University of Rome, 00184 Rome, Italy*

E-mail: konstantinos.pantzas@c2n.upsaclay.fr

This supplement is 11 pages long and contains 4 figures.

Losses and group index

Losses and group indices for TE and TM polarisations are extracted using Fabry-Pérot fringe analysis, following the work in Reference[1]. The experimental setup consists of a broadband light source (Exalos EBS300006-03), the waveguide under study, a polarisation controller to choose either of the two polarisations, and an optical spectrum analyzer (OSA) to record the transmitted spectrum. The normalized transmission spectra for TE and TM are presented in Fig. S1 (a). The losses for each mode, deduced from the fringe contrast and a reflectivity of 0.3 for both cleaved facets, are represented in Fig. S1 (b). Losses for the TE polarisation are less than $10\,\mathrm{cm}^{-1}$ over the entire frequency range in the spectrum, and as low as $7\,\mathrm{cm}^{-1}$ in the region of interest (187 THz to 188.5 THz). Losses for the TM polarisation are similar to those for the TE polarisation, except for a peak of $20\,\mathrm{cm}^{-1}$ at 188 THz. Taking these losses into account, the group index is retrieved from the spectral interval between fringes in the transmitted spectra plotted in Fig. S1 (a). The evolution of the group index for TE and TM as a function of frequency are plotted in Fig. S1 (c). The plots reveal that the group index is slightly higher than the index of GaP (3.05). No difference between TE and TM is observed.

Thermal drift

In an ideal OP-GaP structure and at the considered frequencies, all the input optical-pump power should be converted, transmitted or, back-reflected. In real structures, residual doping, surface states on the etched facets of the waveguide or defects at the bonding and regrowth interfaces, or the inversion boundaries between the alternating domains in OP-GaP can all contribute to losses in these structures. Among these, the last are highly detrimental, as they overlap the most with the optical mode. To better evaluate their individual contribution and

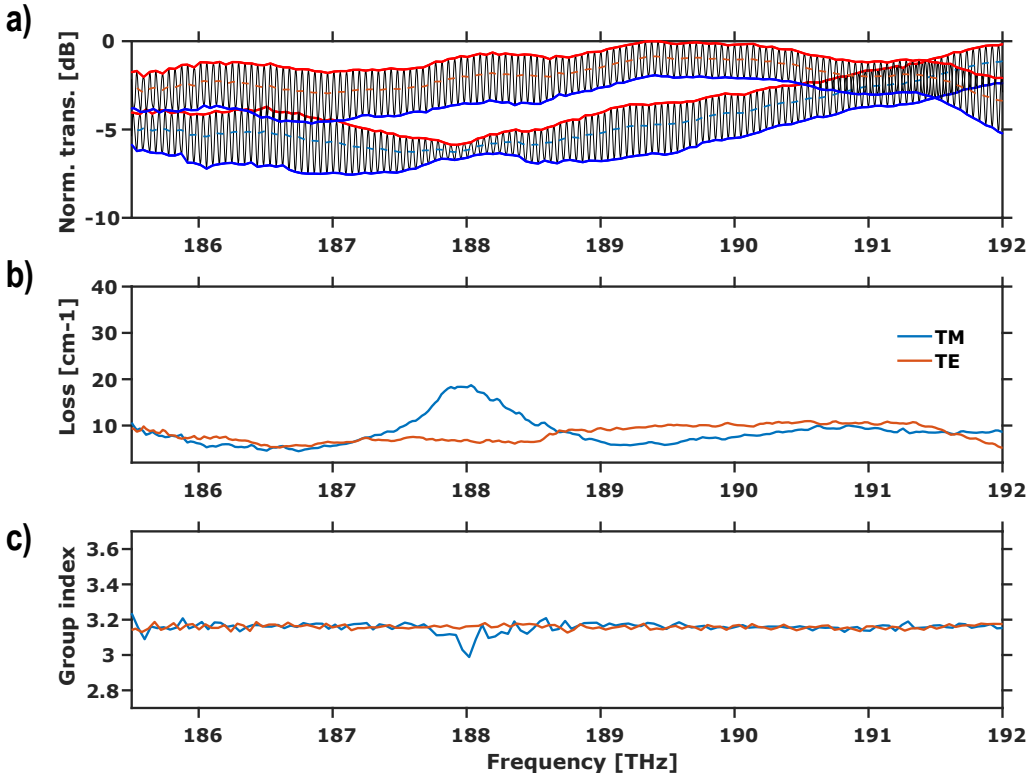

Fig. S1: a) Normalized transmission spectra as a function of frequency for TE and TM polarisation of the fundamental. Envelopes for the two curves are given in red (max) and blue (min). The Fabry-Pérot contrast, computed from these envelopes, is used to deduce losses for TE and TM polarisations. The evolution of these losses as a function of frequency are shown in b). Losses in TE polarisation are less than $10\,\mathrm{cm}^{-1}$ over the entire measured range, and less than $7\,\mathrm{cm}^{-1}$ in the region of interest. Losses in TM polarisation are similar, except for a peak of $20\,\mathrm{cm}^{-1}$ at 188 THz. Taking these losses into account, the Fabry-Pérot fringe spacing is used to deduce the group indices. The evolution of the group index for TE and TM polarisation with frequency is shown in c). The group indices for the two polarisations are similar, and both slightly higher than the optical index of GaP. No TE-TM birefringence on the group index is observed.

discriminate whether their origin lies in scattering or absorption, the percentage of purely optical absorption is deduced from the thermal drift observed in the second-harmonic output power.

The first step in this calculation is to determine the thermal resistance of the suspended waveguide. This resistance can be deduced from the equivalent RC circuit of the waveguide, that follows the equation:

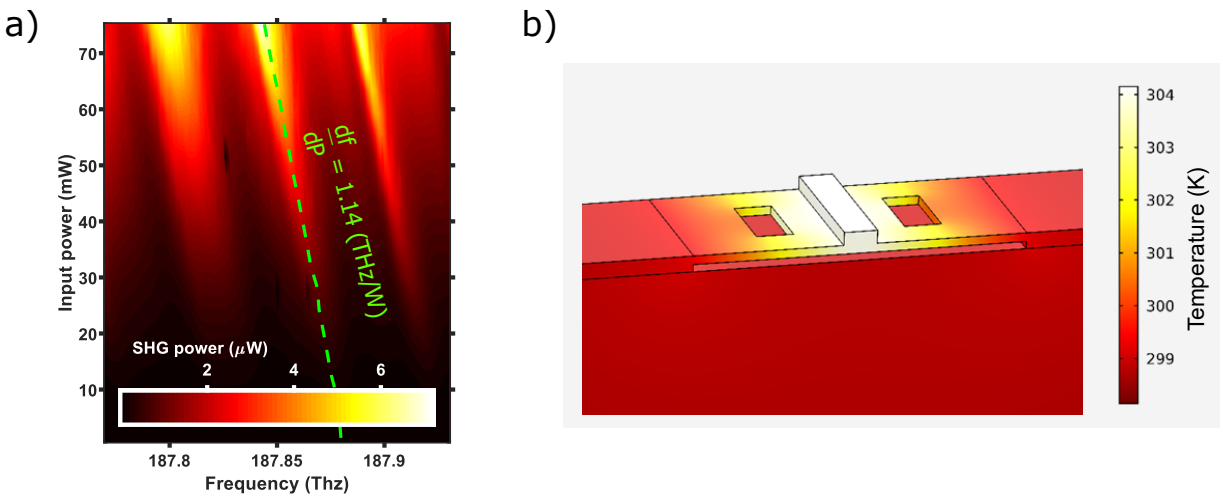

Fig. S2: a) Mapping of the SHG spectra as a function of the incident pump power in the fibre. Spectra are recorded by sweeping the frequency from blue to red and from low to high input power. A frequency drift of the Fabry-Pérot fringes of $1.14\,\mathrm{THz\,W^{-1}}$ is extracted through linear fitting of the maximum generation pic. b) Calculated temperature distribution at steady state of a 20 µm-long suspended waveguide section.

$$C_{\mathrm{th}}\frac{\mathrm{d}T}{\mathrm{d}t} = W - \frac{T}{R_{\mathrm{th}}}. \tag{S1}$$

Here, C_{th} is the circuit's thermal capacity, W the power of the source of heating, and R_{th} the circuit's thermal resistance. The steady-state temperature distribution of a 20 µm-long section of the OP-GaP waveguide is shown in Fig. S2 (a). The distribution was obtained from COMSOL® (Heat transfer in solids model). Only the central part of the modelled section is visible, the complete model being much larger ($H = 350\,\mu\mathrm{m} \times L = 1\,\mathrm{mm} \times W = 20\,\mu\mathrm{m}$) to mimic the real size of the sample. As boundary conditions, an external temperature of 20 °C is imposed on the underside. In the steady state, the left-hand term in Equation S1 is nil, yielding a thermal resistance of $R_{th} = 3.75 \times 10^5\,\mathrm{K\,W^{-1}}$ for the 20 µm-long waveguide. The distribution shows that the side apertures, used to suspend the waveguide, tend to increase the temperature in the waveguide and, hence, the thermal resistance.

In order to determine the fractional power absorbed in the sample, the temperature within the waveguide has to be determined. This is done by recording the conversion efficiencies as

a function of wavelength for increasing input powers. Fig. S2 (a) maps the second-harmonic output power to the incident pump power in the fibre and the frequency of the second harmonic. The mapping reveals the presence of a linear drift of the frequency at peak SHG with increasing input power, with a slope of $1.14\,\mathrm{THz\,W^{-1}}$. This value takes into account 3.75 dB of coupling losses. Considering that $\frac{\Delta f}{f} = \frac{\Delta n}{n}$, an index change of $\Delta n = 5.47 \times 10^{-4}$ is deduced. Differentiating the Sellmeier equation[2] yields a thermo-optical coefficient of $\frac{\Delta n}{\Delta T} = 1.189 \times 10^{-4}\,\mathrm{K^{-1}}$. Thus a 4.6 K temperature increase is deduced. Knowing the average power in the 1 mm-long waveguide, $P = \sqrt{P_{in} * P_{out}}$ =23 mW, and according to Equation S1, we can estimate 2.67 % of the circulating optical power is absorbed, a value that corresponds to an absorption coefficient α of $0.27\,\mathrm{cm^{-1}}$.

Optimal interaction length

Under the hypothesis of a non-depleted pump, the conversion efficiency for second harmonic generation is:

$$\eta = \frac{2\omega^2}{\varepsilon_0 c^3} \frac{d_{\mathrm{eff}}^2}{n_\omega^2 n_{2\omega}} L^2 \mathcal{H} \Gamma. \tag{S2}$$

The optimal waveguide length L_{opt} is defined as the length for which η is maximum. Therefore:

$$\left.\frac{\mathrm{d}\eta}{\mathrm{d}L}\right|_{L=L_{\mathrm{opt}}} = 0. \tag{S3}$$

In Equation S2, only $L^2 h$ depends on L. Hence, Equation S3 can be written as:

$$\left.\frac{\mathrm{d}}{\mathrm{d}L}\left(L^2 \mathcal{H}\right)\right|_{L=L_{\mathrm{opt}}} = 0. \tag{S4}$$

The phase-mismatch function, $\mathcal{H}$ is defined as:

$$\mathcal{H} = \frac{\Big(\sinh\big(\Delta\alpha L/2\big)\cos\big(\Delta\beta L/2\big)\Big)^2 + \Big(\cosh\big(\Delta\alpha L/2\big)\sin\big(\Delta\beta L/2\big)\Big)^2}{\Big(\big(\Delta\alpha^2 + \Delta\beta^2\big)L^2/4\Big)} \times e^{-\left(\frac{a_{2\omega}}{2}+\alpha_\omega\right)L}. \tag{S5}$$

Quasi phase matching implies $\Delta\beta = 0$. As a result, Equation S5 reduces to:

$$\mathcal{H} = \frac{\sinh^2\big(\Delta\alpha L/2\big)}{\Delta\alpha^2 L^2/4} \times e^{-\left(\frac{a_{2\omega}}{2}+\alpha_\omega\right)L}. \tag{S6}$$

Following this equation, $L^2\mathcal{H}$ can be expressed as:

$$L^2\mathcal{H} = \frac{\sinh^2\big(\Delta\alpha L/2\big)}{\Delta\alpha^2/4} \times e^{-\left(\frac{a_{2\omega}}{2}+\alpha_\omega\right)L}. \tag{S7}$$

Using the following identity:

$$\sinh^2(x) = \frac{1}{2}\big(\cosh(2x) - 1\big), \tag{S8}$$

Equation S7 becomes:

$$L^2\mathcal{H} = \frac{\cosh\big(\Delta\alpha L\big) - 1}{\Delta\alpha^2/2} \times e^{-\left(\frac{a_{2\omega}}{2}+\alpha_\omega\right)L}. \tag{S9}$$

By definition, the hyperbolic cosine is:

$$\cosh(x) = \frac{e^x + e^{-x}}{2}. \tag{S10}$$

Using this definition, Equation S9 can be expanded to:

$$L^2\mathcal{H} = \frac{e^{\Delta\alpha L} + e^{-\Delta\alpha L} - 2}{\Delta\alpha^2} \times e^{-\left(\frac{a_{2\omega}}{2}+\alpha_\omega\right)L}. \tag{S11}$$

Carrying the exponential, the last equation further simplifies to:

$$L^2\mathcal{H} = \frac{1}{\Delta\alpha^2}\left(e^{-2\alpha_\omega L} + e^{-2\frac{\alpha_{2\omega}}{2}L} - 2e^{-\left(\frac{a_{2\omega}}{2}+\alpha_\omega\right)L}\right) \tag{S12}$$

Differentiating this expression with respect to L yields:

$$\frac{\mathrm{d}}{\mathrm{d}L}\Big(L^2\mathcal{H}\Big) = \frac{1}{\Delta\alpha^2}\left(-2\alpha_\omega e^{-2\alpha_\omega L} - 2\frac{\alpha_{2\omega}}{2}e^{-2\frac{\alpha_{2\omega}}{2}L} + 2\Big(\frac{a_{2\omega}}{2}+\alpha_\omega\Big)e^{-\left(\frac{a_{2\omega}}{2}+\alpha_\omega\right)L}\right). \tag{S13}$$

The derivative is equal to zero if:

$$-2\alpha_\omega e^{-2\alpha_\omega L} - 2\frac{\alpha_{2\omega}}{2}e^{-2\frac{\alpha_{2\omega}}{2}L} + 2\Big(\frac{a_{2\omega}}{2}+\alpha_\omega\Big)e^{-\left(\frac{a_{2\omega}}{2}+\alpha_\omega\right)L} = 0. \tag{S14}$$

Simplifying by two and factoring terms in α_ω and $\alpha_{2\omega}$ yields:

$$\alpha_\omega\Big(e^{-\left(\frac{a_{2\omega}}{2}+\alpha_\omega\right)L} - e^{-2\alpha_\omega L}\Big) + \frac{\alpha_{2\omega}}{2}\Big(e^{-\left(\frac{a_{2\omega}}{2}+\alpha_\omega\right)L} - e^{-2\frac{\alpha_{2\omega}}{2}L}\Big) = 0. \tag{S15}$$

Factoring out $e^{-\alpha_\omega L}$ in the first parenthesis and $e^{-\frac{\alpha_{2\omega}}{2}L}$ in the second yields:

$$\alpha_\omega e^{-\alpha_\omega L}\Big(e^{-\frac{a_{2\omega}}{2}L} - e^{-\alpha_\omega L}\Big) - \frac{\alpha_{2\omega}}{2}e^{-\frac{a_{2\omega}}{2}L}\Big(e^{-\frac{a_{2\omega}}{2}L} - e^{-\alpha_\omega L}\Big) = 0, \tag{S16}$$

which, in turn, can be factored and rewritten as:

$$\Big(\alpha_\omega e^{-\alpha_\omega L} - \frac{\alpha_{2\omega}}{2}e^{-\frac{a_{2\omega}}{2}L}\Big)\Big(e^{-\frac{a_{2\omega}}{2}L} - e^{-\alpha_\omega L}\Big) = 0. \tag{S17}$$

For $L > 0$ and non-zero absorption losses, the last equation is equivalent to:

$$\alpha_\omega e^{-\alpha_\omega L} - \frac{\alpha_{2\omega}}{2}e^{-\frac{a_{2\omega}}{2}L} = 0. \tag{S18}$$

This, in turn, is equivalent to:

$$e^{\Delta\alpha L} = \frac{\alpha_{2\omega}}{2\alpha_{\omega}}. \tag{S19}$$

Using the natural logarithm and solving for L yields an optimal length L_{opt} of:

$$L_{\mathrm{opt}} = \frac{1}{\Delta\alpha} \ln \frac{\alpha_{2\omega}}{2\alpha_{\omega}}, \tag{S20}$$

or, finally:

$$L_{\mathrm{opt}} = \frac{2}{\alpha_{2\omega} - 2\alpha_{\omega}} \ln \frac{\alpha_{2\omega}}{2\alpha_{\omega}}. \tag{S21}$$

With both α_{ω} and $\alpha_{2\omega}$ at $7\,\mathrm{cm}^{-1}$, L_{opt} has a value of 2 mm, twice the one used in the paper. Therefore, the conversion efficiency can be improved by a factor 1.4 simply by doubling the length of the waveguide. Furthermore, assuming that $\alpha_{\omega} \sim \alpha_{2\omega}$, a reduction by a factor two of the losses would allow increase the optimal length to 4 mm, at which length the conversion efficiency would be $1100\,\%\,\mathrm{W}^{-1}\,\mathrm{cm}^{-2}$, a factor five improvement. Reducing the losses by a factor ten and keeping the length to 4 mm, would yield a conversion efficiency of $6000\,\%\,\mathrm{W}^{-1}\,\mathrm{cm}^{-2}$, better than PPLN waveguides reported in the literature for similar lengths. Fig. S3 shows plot that summarize these findings.

Impact of slanted waveguide sidewalls on Type I and Type II configurations

Overlapping between Type-I and Type-II SHG processes has been observed experimentally. Yet calculations performed using an ideal waveguide profile, do not predict such overlap even though, for reasons related to the almost squared geometry of the waveguide, the two generation maxima are spectrally close. In order to investigate this in more detail, simulations were carried out using FIMMWAVE®. On figure S4a) is reported the period Λ for the quasi-phase matching (QPM) as a function of wavelength for Type-I and Type-II

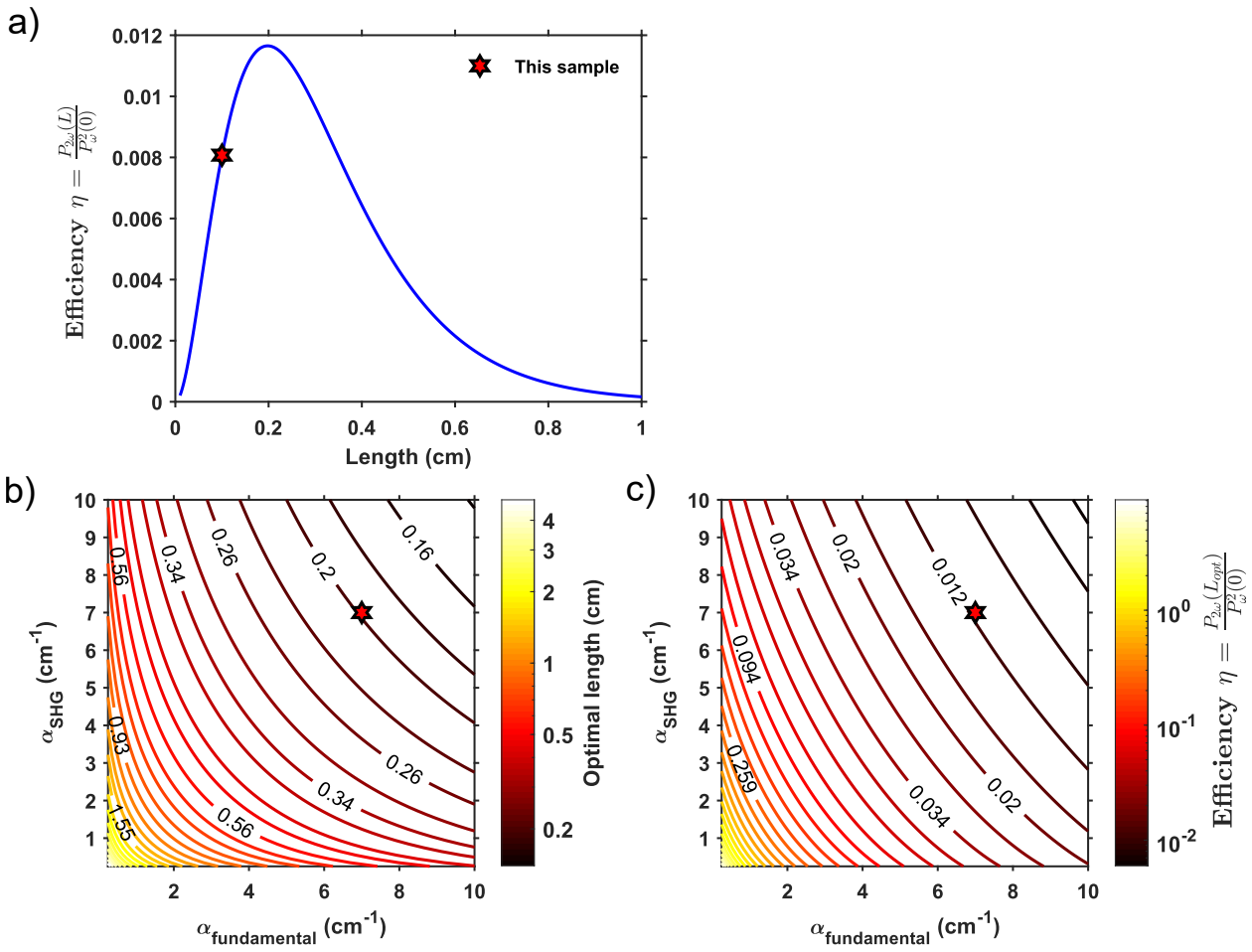

Fig. S3: (a) Conversion efficiency versus waveguide length for losses at 7 cm^{-1}. The optimal length is 2 mm. (b) Optimal length and (c) Conversion efficiency as a function of losses for the fundamental and the second harmonic.

configurations. With respect to experimental data, for a poling period of 5.5 µm, the Type-I and Type-II maximum generation processes are respectively 35 nm and 15 nm off (spectral separation of 20 nm).

Due to a dependence of the etching behavior between the two orientations of GaP, a periodic modulation of the sidewall angle is observed. SEM observations suggest angles of ±15 deg depending on which material orientation is considered (direct or indirect). New calculations were made taking into account this consideration. Note that the width of the waveguide W at the top is kept constant whatever the angle. Effective indices were computed for both angles and then averaged for the two polarisations of the field. On figure S4b), one

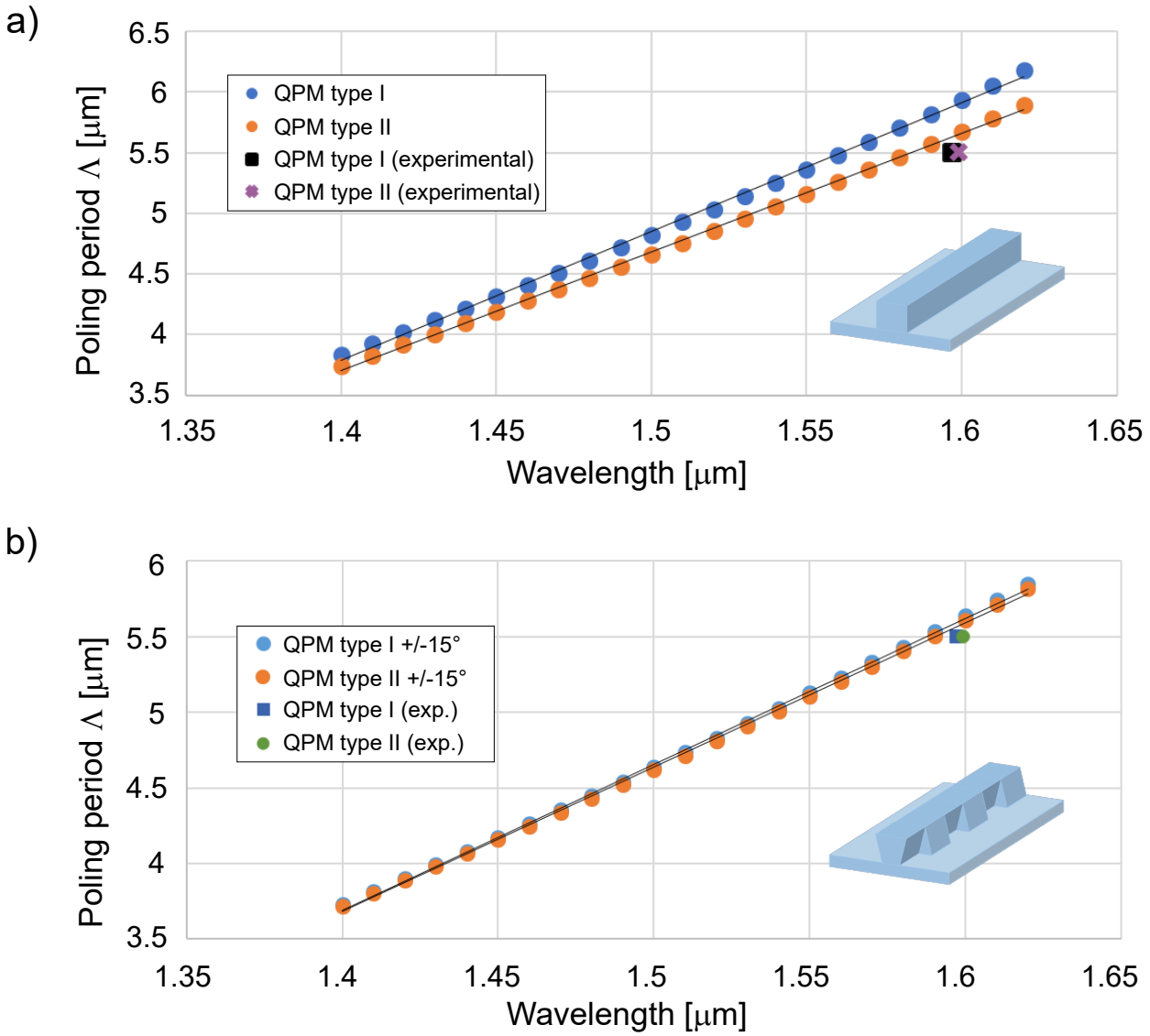

Fig. S4: Period Λ for the quasi-phase matching as a function of wavelength for respectively a) ideal waveguide profile and b) periodically modulated sidewall angles (±15 deg).

can observe that the offset is reduced (≈10 nm off) with respect to experiment and more importantly Type-I and Type-II are now very close with a spectral separation of 2.9 nm (≈350 GHz), in good agreement with the experiment.

References

(1) Combrié, S.; Weidner, E.; DeRossi, A.; Bansropun, S.; Cassette, S.; Talneau, A.; Benisty, H. Detailed analysis by Fabry-Pérot method of slab photonic crystal line-defect waveguides and cavities in aluminium-free material system. *Optics express* **2006**, *14*, 7353–7361.

(2) Wei, J.; Murray, J. M.; Barnes, J. O.; Krein, D. M.; Schunemann, P. G.; Guha, S. Temperature dependent Sellmeier equation for the refractive index of GaP. *Optical Materials Express* **2018**, *8*, 485–490.